Subpicosecond Spectroscopic Ellipsometry of the Photoinduced Phase Transition in VO 2 Thin Films

Yael Gutiérrez, Saúl Vázquez-Miranda, Shirly Espinoza, Krishna Khakurel, Mateusz Rebarz, Zhen Zhang, José Saiz, Shriram Ramanathan, Sébastien Cueff

ACS Photonics

Open Access

pubs.acs.org/journal/apchd5

Article

Subpicosecond Spectroscopic Ellipsometry of the Photoinduced Phase Transition in VO_2 Thin Films

Yael Gutiérrez,* Saúl Vázquez-Miranda, Shirly Espinoza, Krishna Khakurel, Mateusz Rebarz, Zhen Zhang, José M. Saiz, Shriram Ramanathan, and Sébastien Cueff

Cite This: https://doi.org/10.1021/acsphotonics.4c01414

Read Online

ACCESS | Metrics & More | Article Recommendations | Supporting Information

ABSTRACT: We report the first application of broadband time-resolved pump–probe ellipsometry to study the ultrafast dynamics of the photoinduced insulator-to-metal transition (IMT) in vanadium dioxide (VO_2) thin films driven by 35 fs laser pulses. This novel technique enables the direct measurement of the time-resolved evolution of the complex pseudodielectric function of VO_2 during the IMT. We have identified distinct thermal and nonthermal dynamics in the photoinduced IMT, which critically depends on the pump wavelength and fluence, while providing a detailed temporal and spectral phase map. A comparison of the pseudodielectric function of the VO_2 thin film during thermally and photoinduced phase transitions reveals that the primary differences in the IMT pathways occur within the first picosecond after the pump, driven by nonequilibrium dynamics in this ultrafast time scale. The ultrafast spectroscopic ellipsometry introduced in this work offers a complementary probe to study phase changes in condensed matter and emerging photonic device materials.

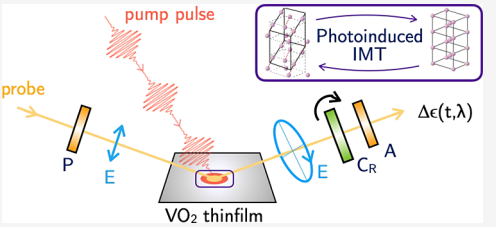

KEYWORDS: *insulator-to-metal transition, vanadium dioxide, ultrafast, pump–probe spectroscopy, spectroscopic ellipsometry*

INTRODUCTION

Vanadium dioxide, VO_2, is a correlated-electron material exhibiting an insulator-to-metal transition (IMT). The transition from an insulating to a metallic state is the result of the collapse of the band gap and formation of a metallic band structure at the IMT temperature, causing drastic changes in the electrical and optical properties of the material. The IMT is accompanied by a structural phase transition (SPT). Below T = 68 °C, VO_2 has monoclinc M crystal symmetry with a semiconducting band structure with a band gap of 0.6 eV.[1] At the IMT temperature of $T \approx 68$ °C, VO_2 undergoes a first-order phase transition to the high temperature rutile R phase. These simultaneous changes of both the electronic structure and crystal lattice make the phase change a rather interesting topic of study across physical sciences and engineering.[2] Although early demonstrations of the IMT were thermally induced, it has been demonstrated that this process can also be driven optically[3] or electrically.[4,5]

Based on this phenomenon, a plethora of devices with reconfigurable optical responses have been proposed in the literature, modulated by either thermal, electrical, and optical stimuli.[2] Among all these devices, of special importance are those related to vanadium dioxide waveguides to be incorporated as on-chip components for photonic integrated circuits aiming to exploit the benefits of light for communication and data processing at the nanoscale.[6−14] In this field, all-optical switching has been proposed as one of the most promising switching schemes. As the IMT can be triggered in subpicosencond time scales,[10−13] it is possible to perform terabits per second (Tbps) on-chip optical switching as recently demonstrated.[13] Nevertheless, the ultrafast optical switching in VO_2 can also be relevant for other applications such as ultrafast wavefront control[2,15,16] or image processing[17] through VO_2 metasurfaces.

Given the potential technological importance of the photoinduced IMT in VO_2, its understanding and the ability to control it are crucial. The photoinduced IMT has a nonthermal basis and therefore occurs on subpicosecond time scales. The evolution and dynamics of this photoinduced IMT have been studied using a wide variety of ultrafast time-resolved techniques (e.g., electron diffraction,[3,18,19] differential transmittance/reflectance,[11,20,21] photoemission,[22,23] etc.) in order to establish the ultrafast electron and lattice dynamics. In these time-resolved experiments, a strong pump pulse is used to excite the system, while a secondary pulse is used to probe a specific property as a function of the time delay between these two pulses. These experiments have demonstrated that during the photoinduced phase transition, the IMT and the SPT do not occur congruently,[24] and metallic transient phases could appear during the process.[20,25−29] An extensive and comprehensive review of the up-to-date knowledge of the mechanism

Received: July 29, 2024
Revised: October 2, 2024
Accepted: October 3, 2024

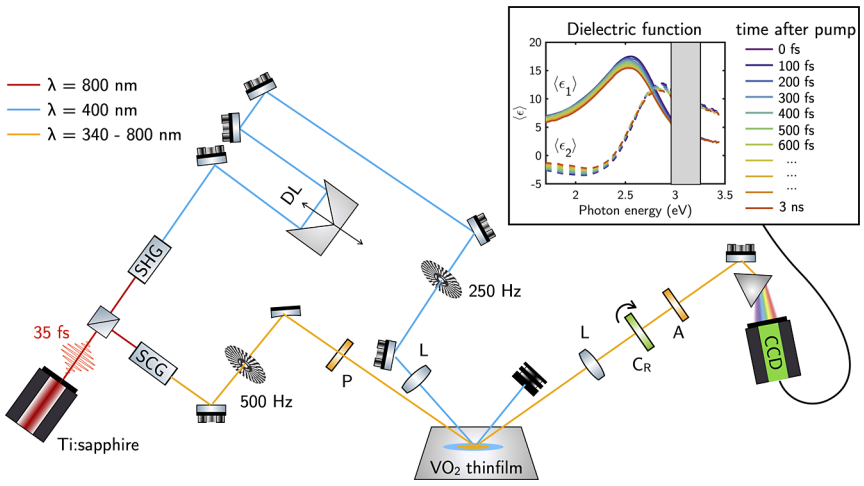

Figure 1. Sketch of the experimental setup for the pump−probe time-resolved spectroscopic ellipsometer. SHG, second harmonic generation for the pump-beam; SCG, supercontinuum white light generation for the probe-beam; DL, delay line; L, lens; P, polarizer; C_R rotating compensator; A, analyzer. The repetition rate of the pump is 250 Hz. This technique allows us to capture the complex pseudodielectric function of the VO_2 thin film as a function of time after the pump, with a temporal resolution of 100 fs, over a broad spectral range from 1.7 to 3.5 eV.

behind the ultrafast IMT has been provided by Wegkamp and Sthäler.[23]

Among time-resolved spectroscopy techniques, broadband time-resolved spectroscopic ellipsometry[30] is a powerful tool for determining the nature of ultrafast dynamics in complex materials and for the study of optically induced phase transitions.[31] With this technique, changes in the complex dielectric function can be measured spectrally as a function of time after pump pulse excitation. Unlike single-wavelength time-resolved reflectance/transmittance measurements[11,20,21]—both techniques widely used to study the laser-induced IMT in VO_2—time-resolved ellipsometry offers the additional possibility of extracting the parametrization of the complex dielectric function over a broad spectral range with a temporal resolution of a few femtoseconds. This emerging time-resolved technique has already been successfully applied to obtain the transient dielectric function of semiconductors and to study the optical properties of such materials after the photoexcitation of carriers,[32−36] as well as to study the photoinduced insulator-to-metal transition in perovskite thin films.[37]

In this work, we exploit the novel technique of broadband time-resolved pump−probe spectroscopic ellipsometry to capture, with 100 fs resolution, the spectral changes in the complex pseudodielectric function of VO_2 thin films during the photoinduced insulator-to-metal transition, as schematized in Figure 1. For the first time to our knowledge, we compare the complex pseudodielectric function of a VO_2 thin film across the IMT driven both thermally and by ultrashort laser pulses. By comparing these two processes, we identified that the primary differences between these pathways occur within the first picosecond after the pump. These differences are attributed to nonequilibrium dynamics. Such ultrafast dynamics have garnered significant attention, as numerous studies[20,25−29] have reported the emergence of transient crystallographic phases in these ultrafast time scales. Additionally, the transient changes in the ellipsometric features are used to obtain characteristics of the photoinduced phase transition such as rise/decay times or threshold fluences to better understand the dynamics of the photoinduced IMT. Moreover, it should be noted that the time-resolved broadband changes in the ellipsometric parameters measured with this technique can be used to fit independently the time-dependent complex pseudodielectric function for any defined pump parameters, thus providing fundamental data sets essential for modeling ultrafast reconfigurable VO_2 optical devices.[38−41]

METHODS

Thin Film Fabrication. VO_2 thin films (25 nm thickness) were deposited on quartz substrates by magnetron sputtering. The thin films exhibit a polycrystalline structure, as confirmed by X-ray diffraction (XRD) analysis. A V_2O_5 target was sputtered at a power of 100 W of radio frequency. During deposition, the substrate was maintained at 750 °C; the chamber pressure was kept at 5 mTorr with flowing of 49.5 sccm Ar and 0.5 sccm 10% Ar-balanced oxygen gases. The thin film XRD was collected in transmission mode using a tube X-ray operated at Copper K-α corresponding to a wavelength of 1.5406 Å.

Temperature-Dependent Spectroscopic Ellipsometry. The complex dielectric function of the VO_2 thin film is analyzed by using a variable-angle spectroscopic ellipsometer (UVISEL, Horiba Jobin-Yvon). The incident broadband light source (xenon lamp) is polarized at 45°. To study temperature-dependent optical properties, measurements are conducted over a temperature range of 30 to 85 °C using a digitally controlled heating stage (Linkam THMSEL350 V). The measured complex pseudodielectric function $\langle\epsilon\rangle = \langle\epsilon_1\rangle + i\langle\epsilon_2\rangle$ of the samples was taken at an angle of incidence of 65° over a spectral range of 0.75−5.00 eV. The pseudodielectric function represents a dielectric function obtained directly from the measured values ellipsometric parameters (Ψ, Δ) and is calculated from an optical model that assumes a semi-infinite flat substrate. This magnitude allows for the comparison of different materials or films under similar measurement conditions, serving as a baseline for comparative studies. Additionally, it is useful for identifying changes in material properties driven by the temperature or ultrashort laser pulses. In our experiements, since no change in the optical properties of the substrate is expected, any observed variations in the pseudodielectric function can be attributed primarily to the VO_2 film. The complex dielectric function $\epsilon = \epsilon_1 + i\epsilon_2$ of the

https://doi.org/10.1021/acsphotonics.4c01414
ACS Photonics XXXX, XXX, XXX−XXX

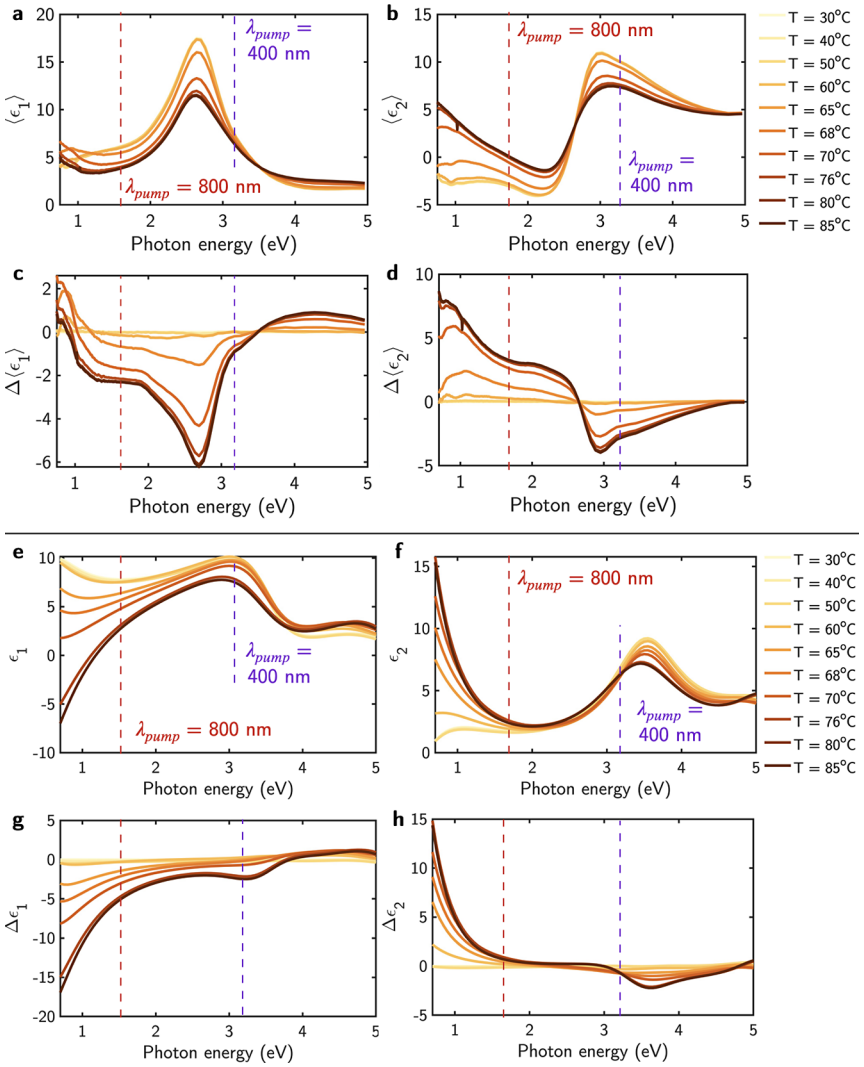

Figure 2. (a) Real and (b) imaginary parts of the pseudodielectric function $\langle\epsilon_1\rangle$ and $\langle\epsilon_2\rangle$ as a function of the temperature of the VO_2 thin film. Changes in the (c) real and (d) imaginary parts of the pseudodielectric function $\Delta\langle\epsilon_1\rangle$ and $\Delta\langle\epsilon_2\rangle$ as a function of the temperature taking the $\langle\epsilon\rangle$ at room temperature as reference. (e) Real and (f) imaginary part of the dielectric function ϵ_1 and ϵ_2 of the VO_2 thin film. Changes in the (g) real and (h) imaginary parts of the pseudodielectric function $\Delta\epsilon_1$ and $\Delta\epsilon_2$ as a function of the temperature taking the ϵ at room temperature as reference. Vertical lines indicate the pump wavelengths λ_{pump} used in the time-resolved ellipsometry experiments.

thin film at different temperatures can be derived by fitting to a realistic multilayer air-VO_2-quartz model of the experimental data.

Time-Resolved Pump−Probe Spectroscopic Ellipsometry. The transient pseudodielectric function was recorded in air using a broadband femtosecond *polarizer-sample-compensator-analyzer* spectroscopic ellipsometer, as described in Richter et al.[30] and schematized in Figure 1. For these experiments, we based the system on the titanium sapphire laser Coherent Astrella, with 800 nm fundamental wavelength that generates a supercontinuum white light pulse in a CaF_2 window and is later filtered by an FGS900-A Thorlabs bandpass filter. The resulting 1.7−3.9 eV broadband pulse was used as the probe pulse with an angle of incidence of 65°. The sample was excited by a pump pulse of 800 nm (1.55 eV) or by its second harmonic corresponding to 400 nm (3.1 eV); its polarization was adjusted by a half waveplate to be *p*-polarized on the sample (i.e., VO_2 thin film), and its angle of incidence was set at 70°, as collinear as possible to the probe pulse. The pump pulse repetition rate was set to 250 Hz to ensure that the film had ample time (4 ms) to fully relax between pulses.[42] Both pump and probe pulses are set to overlap, with the pump pulse having a spot size bigger than the probe to ensure uniform excitation across the probed area. A variable delay line between the pump- and probe beams allows for time-resolved measurements. The data reduction needed for the determination of the pseudo-dielectric was done following the Mueller-Matrix formalism, a chirp correction,[30] and by weighting of the measurements to a steady-state spectrum (Ψ and Δ spectra of the sample before the pump−probe experiment) measured at an EP4 ParkSystem ellipsometer. As a result of the measurement process, we obtain the complex pseudodielectric function of the VO_2 thin film as a function of time after the pump, with a temporal resolution of 100 fs, over a broad spectral range from 1.7 to 3.5 eV. The raw data files from these measurements are available on Zenodo.[43]

https://doi.org/10.1021/acsphotonics.4c01414
ACS Photonics XXXX, XXX, XXX−XXX

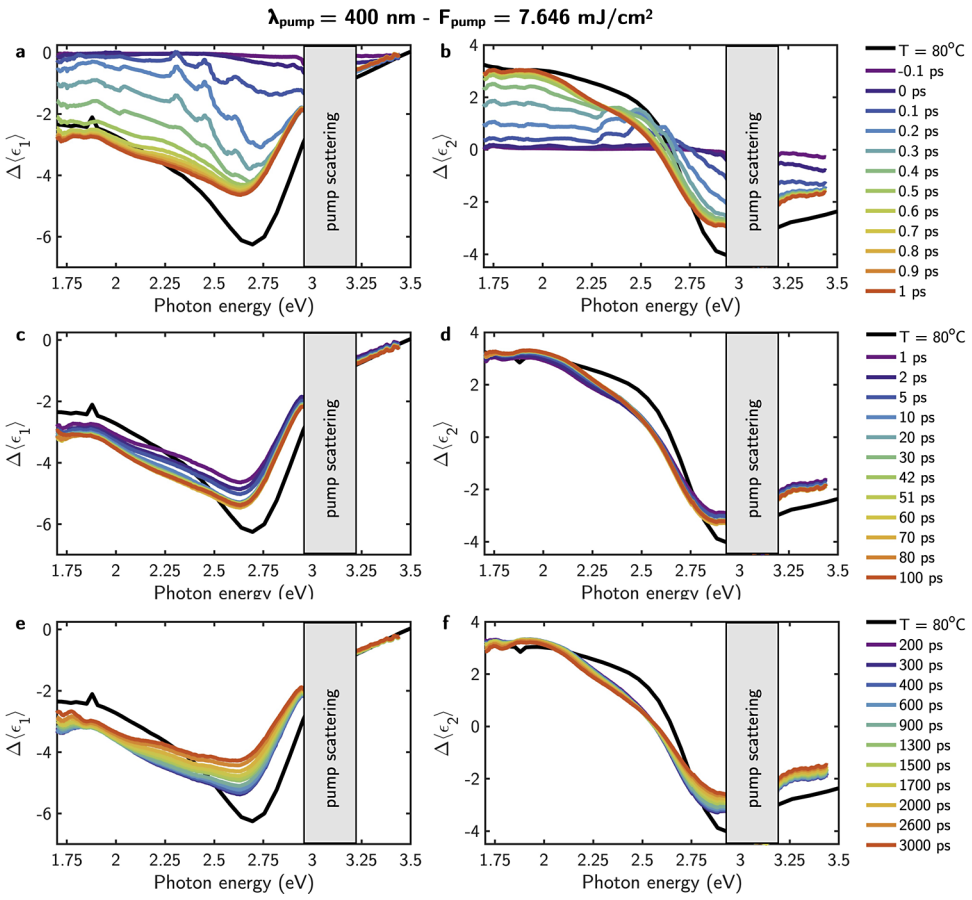

Figure 3. Transient (a, c, e) real and (b, d, f) imaginary part of the pseudodielectric function in the time delay intervals of [−0.1, 1], [1, 100], and [200, 3000] ps. The pump characteristics are λ_{pump} = 400 nm and power = 7.646 mJ/cm^2. As a reference, these plots also show the maximum modulation of $\Delta\langle\epsilon_1\rangle$ and $\Delta\langle\epsilon_2\rangle$ achieved thermally by heating the thin film to T = 80 °C.

RESULTS

We compare the VO_2 thin film optical behavior across the IMT triggered thermally (static) and by ultra short laser pulses (dynamic) to provide a comprehensive analysis of this process.

Thermally Driven IMT: Static Properties. Figure 2a,b shows the pseudodielectric function $\langle\epsilon\rangle = \langle\epsilon_1\rangle + i\langle\epsilon_2\rangle$ of a 25 nm VO_2 thin film deposited on quartz measured with spectroscopic ellipsometry at an angle of incidence of 65° as a function of the temperature in the 30 to 85 °C range. Taking the pseudodielectric function at room temperature (RT) as reference, the changes in $\Delta\langle\epsilon_1\rangle$ and $\Delta\langle\epsilon_2\rangle$ are obtained as a function of the temperature of the film set by a heating stage and are shown in Figure 2c,d. Therefore, $\Delta\langle\epsilon_1\rangle$ and $\Delta\langle\epsilon_2\rangle$ at the different temperatures T are defined as $\Delta\langle\epsilon_1\rangle = \langle\epsilon_1\rangle_T - \langle\epsilon_1\rangle_{RT}$ and $\Delta\langle\epsilon_2\rangle = \langle\epsilon_2\rangle_T - \langle\epsilon_2\rangle_{RT}$. As shown in Figure 2c,d, the values of $\Delta\langle\epsilon_1\rangle$ and $\Delta\langle\epsilon_2\rangle$ are negligible for temperatures $T \leq 60$ °C. At temperatures $T > 68$ °C, the VO_2 thin film is driven across the IMT, and the $\Delta\langle\epsilon_1\rangle$ and $\Delta\langle\epsilon_2\rangle$ increase until reaching a maximum difference at T = 80 °C.[14,44]

To further investigate the optical properties of the thin film, we extract its complex dielectric function by fitting $\epsilon = \epsilon_1 + i\epsilon_2$ to a physically consistent optical model. This model consists of a system composed of air-VO_2-quartz stacked planar layers. Figure 2e,f shows the dielectric function of VO_2 as a function of the temperature. These results align well with the literature, providing a reliable baseline for comparison.[2,44] It can be observed how, as the thin film is heated, ϵ_1 turns negative, and simultaneously, ϵ_2 increases. Variation in the dielectric function with respect to the values obtained at RT is shown in Figure 2g,h. Modifications as large as $\Delta\epsilon = \epsilon_T - \epsilon_{RT} \approx 15$ in the near-IR are reached across the IMT at $T > 68$ °C. The change from $\epsilon_1 > 0$ to $\epsilon_1 < 0$ in this spectral range is indicative of the insulator (dielectric) to metal transition in the thin film. Taking this into consideration, we establish a metallic upper bound for $\Delta\langle\epsilon_1\rangle = -1.95$ at 2 eV as indicative of metallic behavior ($\epsilon_1 < 0$) in the dielectric function of the VO_2 thin film. This reference value is taken from $\Delta\langle\epsilon_1\rangle$ at 2 eV and T = 70 °C, just above the IMT temperature. Therefore, observed values of $\Delta\langle\epsilon_1\rangle < -1.95$ can be associated with the metallic phase of VO_2.

In all plots of Figure 2, vertical lines indicate the pump wavelengths λ_{pump} of 400 (3.1 eV) and 800 nm (1.55 eV) that are used in the time-resolved pump−probe ellipsometry experiments described in the following section.

Photoinduced IMT: Dynamic Properties. The broadband transient pseudodielectric function $\Delta\langle\epsilon\rangle$ of the 25 nm VO_2 thin film was probed in the 1.7 to 3.5 eV range as a function of the fluence and wavelength of the 35 fs pump pulses. The effects of two different pump wavelengths λ_{pump} are compared in this study: λ_{pump} = 400 nm (3.1 eV) and λ_{pump} = 800 nm (1.55 eV). The latter, the most often used λ_{pump} in pump−probe time-resolved spectroscopic studies of VO_2,[3,18,20,21] can be used as reference for comparison with other studies. In particular, it has been reported very recently that the IMT and SPT are decoupled at the subpicosecond time scale upon 800 nm photoexcitation.[24] The photo-

https://doi.org/10.1021/acsphotonics.4c01414
ACS Photonics XXXX, XXX, XXX−XXX

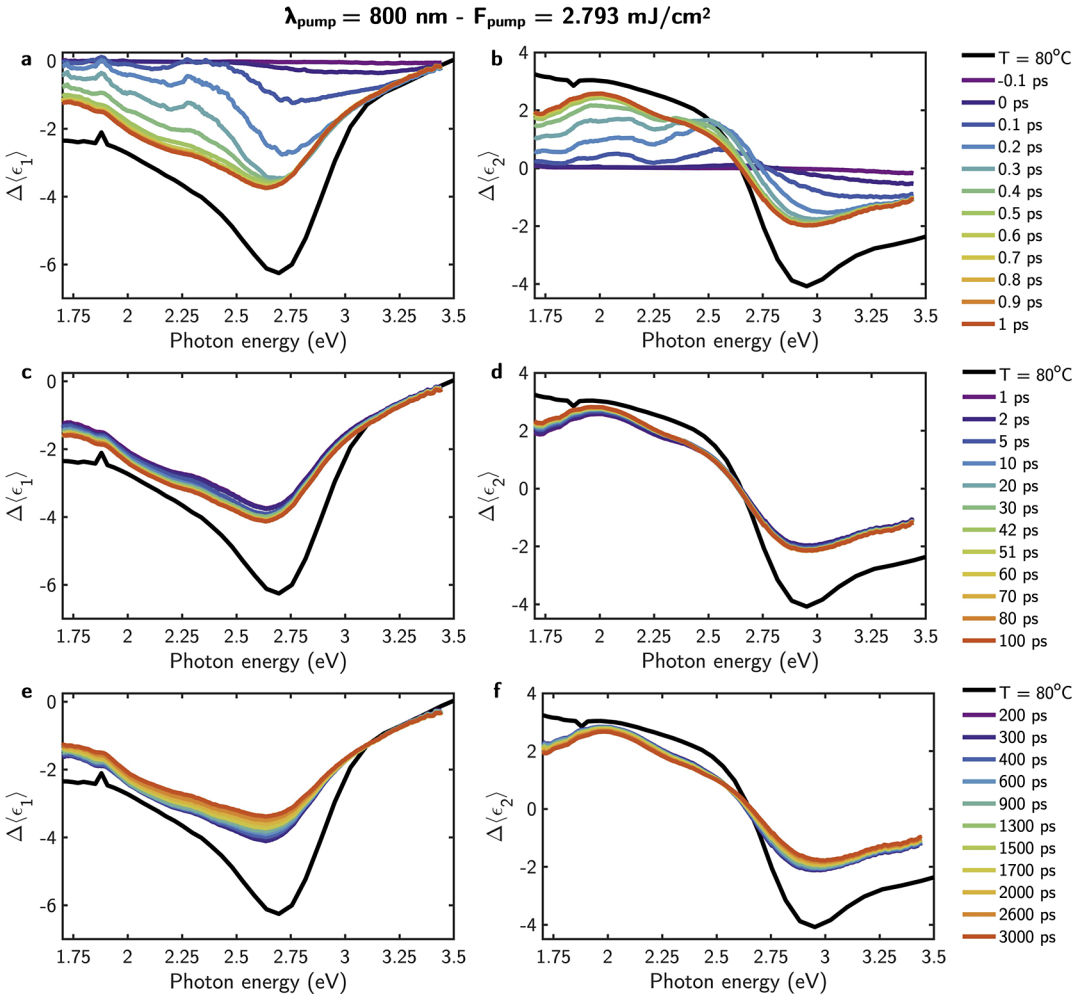

Figure 4. Transient (a, c, e) real and (b, d, f) imaginary parts of the pseudodielectric function in the time delay intervals of [−0.1, 1], [1, 100], and [200, 3000] ps. The pump characteristics are λ_{pump} = 800 nm and power = 2.793 mJ/cm^2. As a reference, these plots also show the maximum modulation of $\Delta\langle\epsilon_1\rangle$ and $\Delta\langle\epsilon_2\rangle$ achieved thermally by heating the thin film to T = 80 °C.

excitation produces holes in the $d_{||}$ valence band, which initiates the dilation of V−V pairs and the increase of twisting angles, driving the structural phase transition from M-VO_2 to R-VO_2. In the case of 400 nm, there is a lack of both experimental and theoretical studies at this pump wavelength; therefore, the excitation mechanism behind the structural M-to-R transition is worth investigating to develop a general framework for photoinduced phase transitions.

For both λ_{pump}, the penetration depth δ_p in the insulating state is greater than the thickness of the film, i.e., δ_p = 68 nm for λ_{pump} = 400 nm and δ_p = 196 nm for λ_{pump} = 800 nm. This ensures that the entire thickness of the VO_2 film is uniformly excited by the pump pulse. The pump fluence F_{pump} used in this study varied between 1.536 and 3.072 mJ/cm^2 for λ_{pump} = 800 nm and from 3.058 to 7.646 mJ/cm^2 for λ_{pump} = 400 nm.

Figures 3 and 4 illustrate the spectral values of $\Delta\langle\epsilon_1\rangle$ and $\Delta\langle\epsilon_2\rangle$ at time delays ranging from 0 to 3000 ps, following excitation with pump pulses of λ_{pump} = 400 nm with F_{pump} = 7.646 mJ/cm^2, and λ_{pump} = 800 with F_{pump} = 2.793 mJ/cm^2, respectively. These plots show the results obtained with the maximum F_{pump} values employed in the experiment, which result in the strongest variation of the optical properties of the VO_2 film. Nevertheless, corresponding plots for the remaining F_{pump} values used in this study are provided in the Supporting Information. Additionally, as a reference, these plots also show the maximum $\Delta\langle\epsilon_1\rangle$ and $\Delta\langle\epsilon_2\rangle$ achieved thermally by heating the thin film to T = 80 °C. Figures 3 and 4 highlight the similarity in the spectral line-shape between the photoinduced $\Delta\langle\epsilon_1\rangle$ and $\Delta\langle\epsilon_2\rangle$ and the thermally induced variation, as presented in Figure 2c,d.

In order to explore how the changes in $\Delta\langle\epsilon_1\rangle$ and $\Delta\langle\epsilon_2\rangle$ synchronize with each other as a function of the F_{pump}, Figure 5 shows evolution of $\Delta\langle\epsilon_1\rangle$ vs $\Delta\langle\epsilon_2\rangle$ monitored at a photon energies E_{probe} = 2 eV and at time delays following the excitation with pump pulses of λ_{pump} = 400 nm and λ_{pump} = 800 nm. Each plot corresponds to a different fluence of the pump pulse. For comparison, the static evolution of these same parameters as a function of the temperature of the film is also shown. Additionally, the vertical dashed line indicates the $\Delta\langle\epsilon_1\rangle$ = −1.95 limit, which allows us to identify metallic and dielectric behavior in the dielectric function of the film. Independently of λ_{pump}, some general trends can be identified:

1. The trajectory of $\Delta\langle\epsilon_2\rangle$ vs $\Delta\langle\epsilon_1\rangle$ during the photoinduced IMT closely aligns with that observed during the static thermally induced transition. However, it is interesting to distinguish two trends in the photoexcitation process of the IMT. Within the first picosecond following the pump, the trajectory of

https://doi.org/10.1021/acsphotonics.4c01414
ACS Photonics XXXX, XXX, XXX−XXX

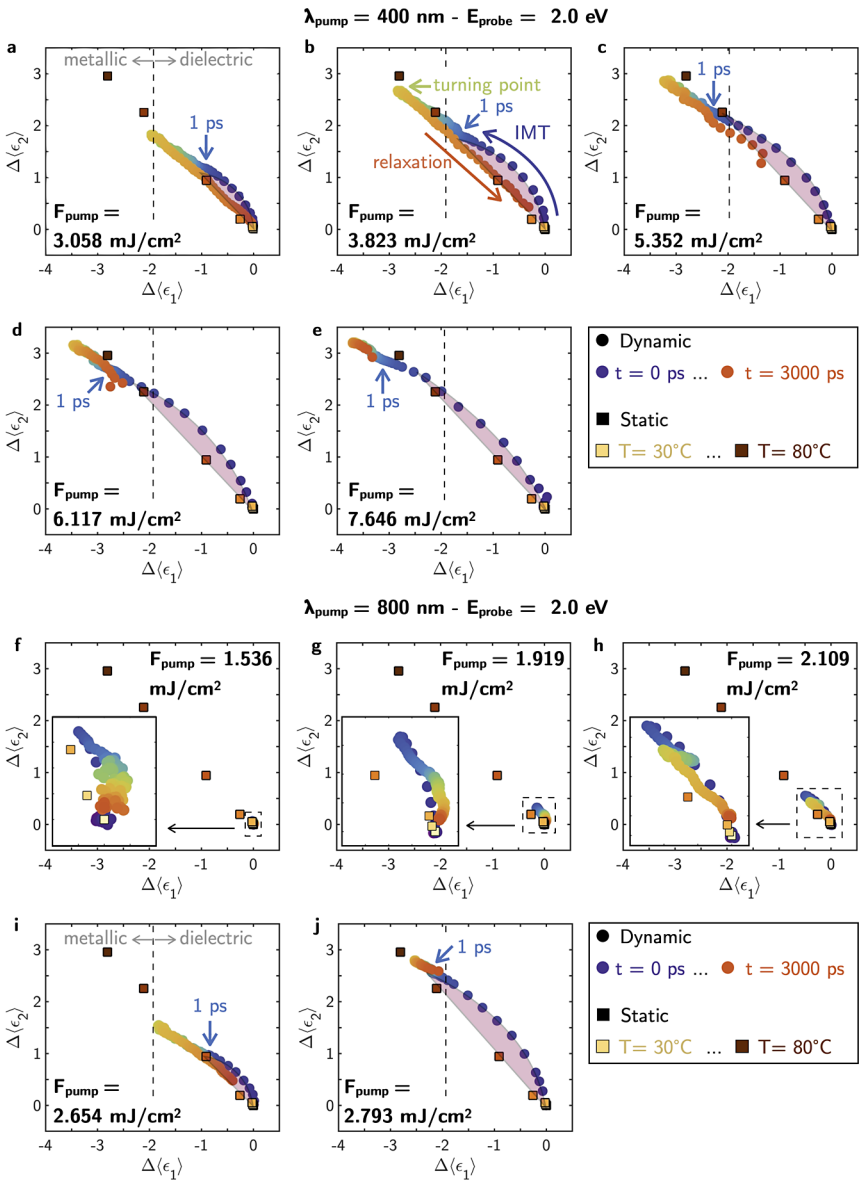

Figure 5. Dynamic $\Delta\langle\epsilon_2\rangle$ vs $\Delta\langle\epsilon_1\rangle$ as a function of delay time t at E_{probe} = 2 eV for pump wavelengths (a–e) λ_{pump} = 400 nm and (f–j) λ_{pump} = 800 nm. Each plot corresponds to a different pump fluence F_{pump}. For comparison, it is shown the static $\Delta\langle\epsilon_2\rangle$ vs $\Delta\langle\epsilon_1\rangle$ at E_{probe} = 2 eV as a function of the temperature of the film T. The vertical dashed line indicates the $\Delta\langle\epsilon_1\rangle = -1.95$ limit, which allows us to identify metallic and dielectric behavior in the dielectric function of the film. The purple shadowed regions highlights the difference between the thermal and photoinduced IMT paths.

$\Delta\langle\epsilon_2\rangle$ vs $\Delta\langle\epsilon_1\rangle$ displays the most pronounced deviation from the thermal path. This first picosencond is of great interest because of the dominance of nonequilibrium dynamics that leads to novel physical phenomena. The discrepancy between nonthermal and thermal paths, highlighted with a purple shadow in Figure 5, may arise from the dominance of nonequilibrium dynamics in which strong electronic excitation, according to Cocker et al.,[29] results in the photoexcited electron-assisted nucleation of the rutile phase (nonthermal process). Other authors have also reported the emergence of short-lived (few hundreds of picoseconds) transient phases after the pump.[20,25−29] After 1 ps, the photoinduced and thermal paths achieve good overlap until reaching a turning point in the $\langle\epsilon_2\rangle$ vs $\langle\epsilon_1\rangle$ trajectory. During this time, the energy of the laser pulse is converted into lattice heating, and thus, the comparatively slower growth of the metallic rutile phase.[29] At higher delay times than the turning point, the relaxation back to the insulating state takes place. During this relaxation process, which is mediated by the cooling of the film, the trajectory of $\Delta\langle\epsilon_2\rangle$ vs $\Delta\langle\epsilon_1\rangle$ closely follows the thermal transition path. This described behavior can be clearly seen in Figure 5b, where each process (IMT and relaxation) and characteristic point (1 ps and turning point) are indicated.

2. This behavior in the values of $\Delta\langle\epsilon_1\rangle$ and $\Delta\langle\epsilon_2\rangle$, which do not follow the same trajectory during excitation and relaxation, leads to an hysteresis effect in the transient pseudodielectric function.
3. The amplitude of $\Delta\langle\epsilon_1\rangle$ and $\Delta\langle\epsilon_2\rangle$ increases with the fluence of the pump independently of λ_{pump}. In the case of λ_{pump} = 400 nm, for all the analyzed F_{pump}, the metallic pseudodielectric function in the film is achieved. On the

https://doi.org/10.1021/acsphotonics.4c01414
ACS Photonics XXXX, XXX, XXX−XXX

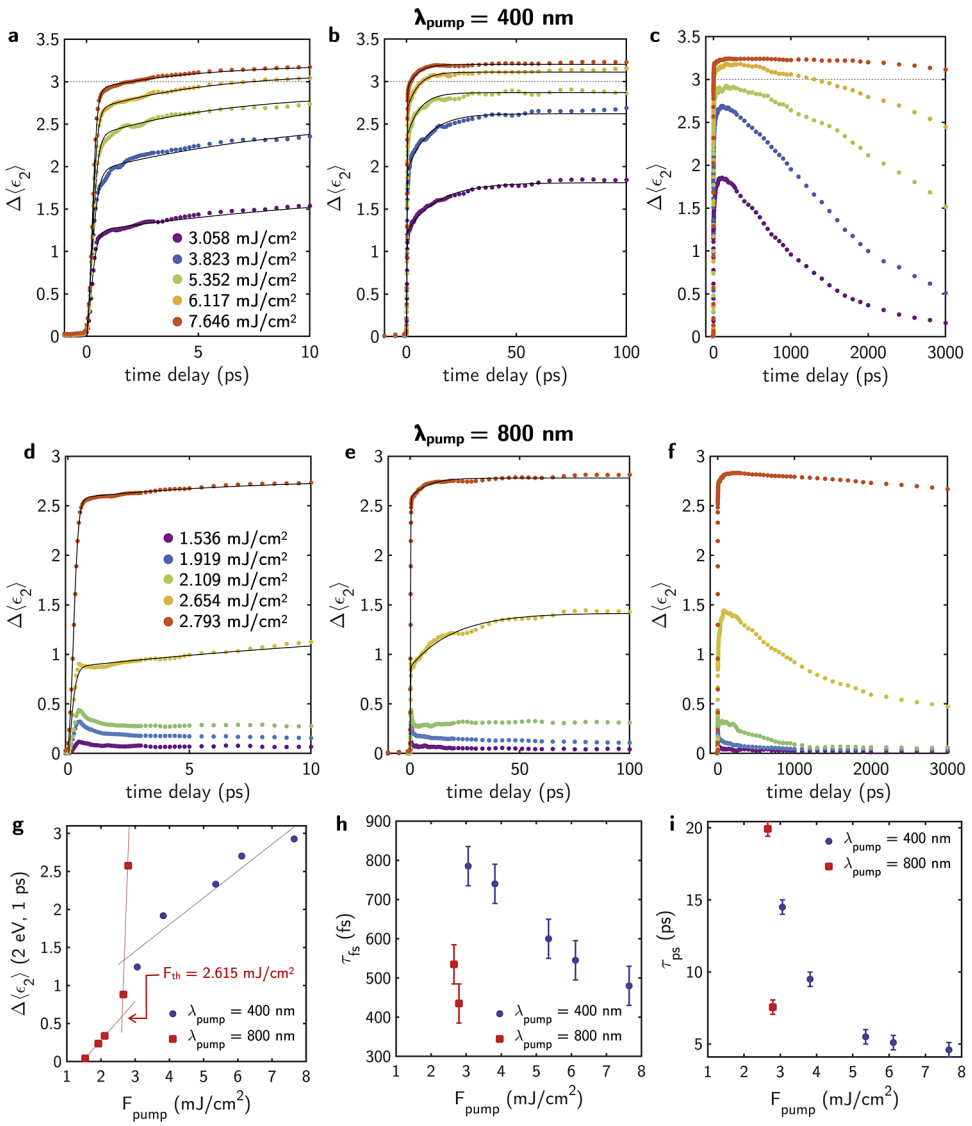

Figure 6. Time-resolved $\Delta\langle\epsilon_2\rangle$ at 2 eV of the VO_2 thin film at different time scales for pump wavelengths of (a−c) λ_{pump} = 400 nm and (d−f) λ_{pump} = 800 nm. In (a−c), a horizontal dashed line indicates the $\Delta\langle\epsilon_2\rangle$ observed for the fully metallic state at 80 °C. For each λ_{pump}, the photoinduced $\Delta\langle\epsilon_2\rangle$ is shown for five pump fluences. Dots indicate the measured experimental data, and the solid lines represent results of fitting the data. (g) Value of $\Delta\langle\epsilon_2\rangle$ measured at 2 eV and delay time of 1 ps as a function of the pump fluence for λ_{pump} = 400 nm and λ_{pump} = 800 nm. Rise times for the (h) short τ_{fs} and (i) long-lived τ_{ps} behavior are extracted from the fitting to the model in eq 1.

contrary, in the case of λ_{pump} = 800 nm, for F_{pump} lower than 2.654 mJ/cm^2, the limit in $\Delta\langle\epsilon_1\rangle$ for the metallic behavior is not reached. Therefore, in the case of λ_{pump} = 800 nm, a fluence threshold for the photoinduced IMT can be defined. On the contrary, for λ_{pump} = 400 nm, all the measurements are performed above that threshold.

4. Increasing F_{pump} not only amplifies the modulation in the optical response of the film but also extends the recovery time to the initial insulating state. This behavior is consistent with the literature.[9]

The main difference between λ_{pump} = 400 nm and λ_{pump} = 800 nm is related to the fluence dependence of $\Delta\langle\epsilon_1\rangle$ vs $\Delta\langle\epsilon_2\rangle$. In order to address this issue and provide with the photoinduced IMT temporal dynamics, Figure 6 shows the time-resolved $\Delta\langle\epsilon_2\rangle$ of the 25 nm VO_2 thin film probed at E_{probe} = 2 eV after excitation by λ_{pump} 400 and 800 nm pump pulses for the five different pump fluences, as shown in Figure 5.

In order to drive the photoinduced IMT, the fluence of the pump pulse should be higher than a certain threshold F_{th}.[20] Below F_{th}, no phase transition occurs, and the material remains in the insulating state. However, in this regime, some authors, based on time-dependent reflectance[25]/transmittance[26] and THz conductivity[27−29] measurements, have reported a transient metallic phase that decays to near initial conditions on a time scale of 2−5 ps and that results from a coherent phonon excitation.[13] Above the threshold, only a small region of the sample is initially transformed to the metallic phase and the dynamics are slow, being governed by heat diffusion into the sample, which results in the growth of the metallic phase.[20,45] Nevertheless, as the F_{pump} increases, the transition occurs more rapidly until it reaches a saturation point, suggesting that nonthermal processes can also drive the structural changes.[3]

Figure 6a−c shows the time-resolved $\Delta\langle\epsilon_2\rangle$ for a λ_{pump} = 400 nm and pumping energies between 3.058 and 7.646 mJ/cm^2.

https://doi.org/10.1021/acsphotonics.4c01414
ACS Photonics XXXX, XXX, XXX−XXX

All the curves show a similar profile consisting of a fast sharp increase of $\Delta\langle\epsilon_2\rangle$ followed by a long-lived slow rise of the signal. To investigate the process, the rise response function of $\Delta\langle\epsilon_2\rangle$ at $t \geq 0$ was phenomenologically fitted to

$$\Delta\langle\epsilon_2\rangle(t) = \Theta(t) - A_0 e^{-t/\tau_{ps}} \quad (1)$$

where $\Theta(t) = \frac{A_1}{1 - e^{-\alpha(t-\beta)}}$ represents a logistic sigmoidal function. A_0, A_1, α, and β are fitting parameters. The sigmoidal function describes a fast nonthermal process which is ascribed to the photoinduced nucleation of the metallic phase.[29] The rise time τ_{fs} of this nonthermal process is defined as the time it takes for the $\Theta(t)$ function to go from 10 to 90% of its maximum value. The exponential term in eq 1 describes a slower process with rise time τ_{ps} ascribed to the thermally driven growth and coalescence of metal domains in the material.[29]

According to the fitting, photoinduced nucleation and growth dynamics consistent with excitation above F_{th} are observed in Figure 6a,b. The values τ_{fs} and τ_{ps} extracted from the fitting, plotted as a function of the pump fluence in Figure 6h,i, show that both τ_{fs} and τ_{ps} decrease with increasing F_{pump}. Therefore, as F_{pump} increases, the photoinduced nucleation and subsequent growth of the metallic domains occur faster. This is also visible in Figure 5a−e, which shows how the limit indicative of metallic behavior in ϵ_1 is reached at shorter time delays for increasing F_{pump}. Additionally, Figure 6g shows that the value of $\Delta\langle\epsilon_2\rangle$, 1 ps after the pump at 2 eV, follows a linear increase with the pump fluence, supporting an above F_{th} regime for all explored F_{pump}. This linear increase of $\Delta\langle\epsilon_2\rangle$ with F_{pump} implies that an increasing volume fraction of the VO_2 thin film converts into the metallic state.

Notably, at higher pump fluences, τ_{ps} stabilizes at its lowest value, which is accompanied by the highest values of $\Delta\langle\epsilon_2\rangle$ at 1 ps, which indicates that the transition to the metallic state is dominated by nonthermal mechanisms, reaching the above F_{th} saturation regime. This is particularly evident for pump fluences of 6.117 and 7.646 mJ/cm^2. As shown in Figure 6a,b, for these pump fluences, $\Delta\langle\epsilon_2\rangle$ reaches values higher than those obtained thermally after approximately 2 and 10 ps, respectively. Additionally, Figure 5d,e demonstrates that the photoinduced IMT path surpasses the thermal path in about 1 ps, supporting the dominating nonthermal behavior associated with the fast photoexcited-electron-assisted nucleation of the rutile phase.

The response of the film was monitored until 3000 ps (3 ns) after the pump, as shown in Figure 6c. This allowed us to analyze recovery times of the initial insulating state. It is possible to observe that the recovery time increases with the pump fluence. In all the analyzed cases, the time for the full recovery of the monoclinic phase is higher than 3 ns. For instance, the recovery of 80% of the signal is achieved after 2 and 3 ns for F_{pump} = 3.058 and 3.823 mJ/cm^2. For the rest of the analyzed F_{pump} at λ_{pump} = 400 nm, these values exceed our 3 ns measurement range.

Figure 6d−f shows the time-resolved $\Delta\langle\epsilon_2\rangle$ for λ_{pump} = 800 nm and pump fluences between 1.536 and 2.793 mJ/cm^2. In this case, measurements with higher F_{pump} than ≈2.793 mJ/cm^2 produced irreversible damage to the film. In the studied range of F_{pump}, two types of dynamics can be seen. On the one hand, for pump fluences ≥2.654 mJ/cm^2, the profile $\Delta\langle\epsilon_2\rangle$ consists of a fast sharp increase of $\Delta\langle\epsilon_2\rangle$ followed by a long-lived slowly rising similar to that observed for λ_{pump} = 400 nm in the F_{pump} range 3.058 to 7.646 mJ/cm^2. However, for λ_{pump} = 800 nm, this regime is observed in a narrower pump fluence window. The dynamics were fitted to eq 1 to extract the values of τ_{fs} and τ_{ps}. As in the case of λ_{pump} = 400 nm, both τ_{fs} and τ_{ps} decrease with an increase in pump fluence. It is noteworthy that values of τ_{fs} in the case of λ_{pump} = 800 nm are lower, indicating a faster photoinduced nucleation of the metallic phase in the VO_2 film. The values of τ_{ps} show a stronger variation with the pumping fluence than in the case of λ_{pump} = 400 nm, suggesting that the growth velocity has a stronger dependence on the pump fluence. In Figure 6f, which shows the dynamics up to 3000 ps after the pump, it can be seen how the recovery times to the full monoclinic phase for pump fluences ≥2.654 mJ/cm^2 also exceed 3 ns.

For pump fluences ≤2.109 mJ/cm^2, the dynamics in Figure 6d−f show a different behavior. The pump fluence threshold in the change of dynamics has been estimated to $F_{th} \approx 2.615$ mJ/cm^2 by the change in the slope of the dependence of $\Delta\langle\epsilon_2\rangle$ 1 ps after the pump at 2 eV as a function of the pump fluence, as shown in Figure 6g. This value agrees well in order of magnitude with other values reported in the literature, although the absolute value appears to be dependent on the thickness of the film with a threshold fluence higher for thicker films (6.1 mJ/cm^2 for 200 nm VO_2 thin film[20]).

Below the threshold fluence, the $\Delta\langle\epsilon_2\rangle$ profile exhibits rapid peak switching with an elevated background after the switching is completed. Similar changes in transient reflectance and transmittance measurements have been associated with a transient metallic state.[13,25,26] However, in the spectral range analyzed here, for these F_{pump}, the pseudodielectric function does not exhibit a metallic behavior, as shown in Figure 5f−h. Interestingly, the recovery time of the $\Delta\langle\epsilon_2\rangle$ in the ≤2.109 mJ/cm^2 pump fluence range is lower than in the above F_{th} regime. In particular, after 1 ns, between 80 and 85% of the signal is recovered. Therefore, in the below F_{th} regime, although we can achieve a lower variation of the pseudodielectric function of the film, the recovery times are fast, making this regime interesting to consider further for optical communications applications.[11,13]

Finally, it should be noted that the lifetime of VO_2 switching performance at high pulse repetition frequency has been identified as an important issue.[13] In the case of photoinduced IMT, very recently, it has been reported the record of 10^7 cycles without degradation in 3 μm long and 40 nm thick VO_2 patches on Si waveguides using pulses of 100 ns and wavelength 1550 nm with a frequency of 10 kHz.[46] In our experiments, for both λ_{pump} = 400 nm and λ_{pump} = 800 nm, each of the presented time-resolved pump−probe ellipsometric measurements requires 3×10^7 pump pulses. This number is derived from the product of the measurement duration and the pump repetition rate. Therefore, we demonstrate here an endurance lifetime of at least 3×10^7 cycles in a 25 nm VO_2 thin film induced by 35 fs pulses with a repetition rate of 250 Hz for λ_{pump} and F_{pump} used in this study.

CONCLUSIONS

This study presents the first broadband time-resolved pump−probe spectroscopic ellipsometry measurements of the photoinduced IMT in VO_2 films. By employing this technique, we capture the complex pseudodielectric function of the VO_2 thin film during the photoinduced IMT with a temporal resolution of 100 fs across a broad spectral range from 1.7 to 3.5 eV. The changes in the optical properties during the photoinduced

https://doi.org/10.1021/acsphotonics.4c01414
ACS Photonics XXXX, XXX, XXX−XXX

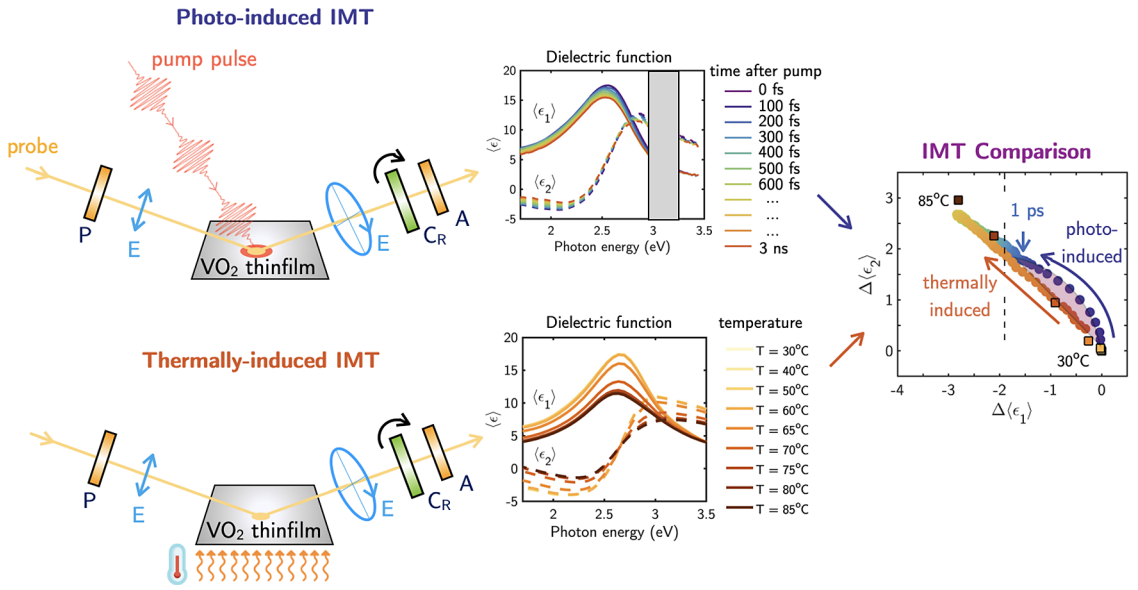

Figure 7. Schematic summary of the ellipsometric measurements performed in this work to capture the pseudodielectric function of a VO_2 thin film across the photoinduced and thermally induced IMT. In the case of the photoinduced IMT, the pseudodielectric function is obtained as a function of the time after pump pulse. For the thermally induced IMT, the pseudodielectric function is measured as a function of temperature. The comparison between both IMT pathways reveals that the most pronounced discrepancies occur within the first picosecond after the pump, as highlighted by the purple shadow.

IMT have been directly compared to those during the thermally activated IMT, offering a comprehensive spectral and temporal mapping of the photoinduced IMT, as schematized in Figure 7. A direct comparison of the complex pseudodielectric function values across the IMT for thermal and laser-induced pathways reveals that the most pronounced discrepancies occur within the first picosecond after the pump driven by nonequilibrium dynamics in this ultrafast scale (shadowed region in Figure 7).

In our experiments, by employing 35 fs pump pulses at two distinct wavelengths (λ_{pump} = 400 and 800 nm) with varied fluences, we discerned diverse thermal and nonthermal dynamics governing the excitation and relaxation of the photoinduced IMT. We identified two types of behavior depending on the fluence of the pump according to what has been reported in the literature. Below a certain fluence threshold, no metallic phase is observed, although a transient in the pseudodielectric function is observed with a relaxing time (≈1 ns). Above the threshold, the observed dynamics are consistent with an initial fast (below 1 ps) nonthermal photoinduced nucleation of the metallic phase, a subsequent slow growth of the metallic domains governed by thermal diffusion, and relatively long relaxing times (>3 ns) to the insulating phase.

Additionally, under our experimental conditions, we report a cycle lifetime of at least 3×10^7 cycles, aligning well with record photoinduced IMT cyclability reported by Seoane et al.[46] These findings not only deepen our comprehension of the ultrafast dynamics intrinsic to the IMT in VO_2 films but also underscore the utility of time-resolved pump−probe spectroscopic ellipsometry as an effective tool for investigating phase transitions in strongly correlated materials. Furthermore, time-resolved pump−probe ellipsometry offers an avenue for independent evaluation of complex dielectric function with defined pump parameters that is essential to guide the applications of phase change materials in emerging photonic device technologies.

■ ASSOCIATED CONTENT

Data Availability Statement

The data underlying this study are openly available at Zenodo.[43]

Supporting Information

The Supporting Information is available free of charge at https://pubs.acs.org/doi/10.1021/acsphotonics.4c01414.

Transient pseudodielectric function in the time delay intervals of [−0.1, 1], [1, 100], and [500, 3000] ps for λ_{pump} = 400 nm and F_{pump} = 3.058, 3.823, 5.352, and 6.117 mJ/cm^2; transient pseudodielectric function in the time delay intervals of [−0.1, 1], [1, 100], and [500, 3000] ps for λ_{pump} = 800 nm and F_{pump} = 1.536, 1.919, 2.109, and 2.654 mJ/cm^2 (PDF)

■ AUTHOR INFORMATION

Corresponding Author

Yael Gutiérrez − *Departamento de Física Aplicada, Universidad de Cantabria, 39005 Santander, Spain; ICMATE, CNR, Istituto di Chimica della Materia Condensata e delle Tecnologie per l'Energia, 35127 Padova, Italy;* orcid.org/0000-0002-1604-7968; Email: gvelay@unican.es

Authors

Saúl Vázquez-Miranda − *ELI Beamlines Facility, The Extreme Light Infrastructure ERIC, 25241 Dolní Břežany, Czech Republic*

Shirly Espinoza − *ELI Beamlines Facility, The Extreme Light Infrastructure ERIC, 25241 Dolní Břežany, Czech Republic*

Krishna Khakurel − *ELI Beamlines Facility, The Extreme Light Infrastructure ERIC, 25241 Dolní Břežany, Czech Republic*

Mateusz Rebarz − *ELI Beamlines Facility, The Extreme Light Infrastructure ERIC, 25241 Dolní Břežany, Czech Republic*

https://doi.org/10.1021/acsphotonics.4c01414
ACS Photonics XXXX, XXX, XXX−XXX

Zhen Zhang − *School of Materials Engineering, Purdue University, West Lafayette, Indiana 47907, United States*
José M. Saiz − *Departamento de Física Aplicada, Universidad de Cantabria, 39005 Santander, Spain*
Shriram Ramanathan − *School of Materials Engineering, Purdue University, West Lafayette, Indiana 47907, United States;* orcid.org/0000-0002-6685-6798
Sébastien Cueff − *Ecole Centrale de Lyon, CNRS, INSA Lyon, Université Claude Bernard Lyon 1, CPE Lyon, CNRS, INL, UMR5270, Université Lyon, 69130 Ecully, France;* orcid.org/0000-0002-8668-2633

Complete contact information is available at: https://pubs.acs.org/10.1021/acsphotonics.4c01414

Funding
Y.G. acknowledges the support from the European Union's Horizon 2020 research and innovation program (No 899598 - PHEMTRONICS) and funding from a Ramon y Cajal Fellowship (RYC2022-037828-I). S.R. acknowledges AFOSR grant FA9550-18-1-0250 for support. S.C. acknowledges funding from the French National Research Agency (ANR) under the project MetaOnDemand (ANR-20-CE24-0013). S.E, S.V.-M., and M.R. acknowledge the project ADONIS (No. CZ.02.1.01/0.0/0.0/16-019/0000789).

Notes
The authors declare no competing financial interest.

■ ACKNOWLEDGMENTS
All authors further acknowledge ELI Beamlines in Dolní Břežany, Czech Republic, for providing beamtime and thank the instrument group and facility staff for their assistance.

■ REFERENCES
(1) Verleur, H. W.; Barker, A. S.; Berglund, C. N. Optical Properties of VO_2 between 0.25 and 5 eV. *Phys. Rev.* **1968**, *172*, 788−798.
(2) Cueff, S.; John, J.; Zhang, Z.; Parra, J.; Sun, J.; Orobtchouk, R.; Ramanathan, S.; Sanchis, P. VO_2 nanophotonics. *APL Photonics* **2020**, *5*, 110901.
(3) Cavalleri, A.; Tóth, C.; Siders, C. W.; Squier, J. A.; Ráksi, F.; Forget, P.; Kieffer, J. C. Femtosecond Structural Dynamics in VO_2 during an Ultrafast Solid-Solid Phase Transition. *Phys. Rev. Lett.* **2001**, *87*, No. 237401.
(4) Sood, A.; Shen, X.; Shi, Y.; Kumar, S.; Park, S. J.; Zajac, M.; Sun, Y.; Chen, L.-Q.; Ramanathan, S.; Wang, X.; Chueh, W. C.; Lindenberg, A. M. Universal phase dynamics in VO_2 switches revealed by ultrafast operando diffraction. *Science* **2021**, *373*, 352−355.
(5) Stefanovich, G.; Pergament, A.; Stefanovich, D. Electrical switching and Mott transition in VO_2. *J. Phys.: Condens. Matter* **2000**, *12*, 8837−8845.
(6) Briggs, R. M.; Pryce, I. M.; Atwater, H. A. Compact silicon photonic waveguide modulator based on the vanadium dioxide metal-insulator phase transition. *Opt. Express* **2010**, *18*, 11192.
(7) Sanchez, L.; Lechago, S.; Gutierrez, A.; Sanchis, P. Analysis and Design Optimization of a Hybrid VO_2/Silicon 2 × 2 Microring Switch. *IEEE Photonics Journal* **2016**, *8*, 1−9.
(8) Joushaghani, A.; Jeong, J.; Paradis, S.; Alain, D.; Stewart Aitchison, J.; Poon, J. K. S. Wavelength-size hybrid Si-VO_2 waveguide electroabsorption optical switches and photodetectors. *Opt. Express* **2015**, *23*, 3657.
(9) Markov, P.; Marvel, R. E.; Conley, H. J.; Miller, K. J.; Haglund, R. F.; Weiss, S. M. Optically Monitored Electrical Switching in VO_2. *ACS Photonics* **2015**, *2*, 1175−1182.
(10) Ryckman, J. D.; Hallman, K. A.; Marvel, R. E.; Haglund, R. F.; Weiss, S. M. Ultra-compact silicon photonic devices reconfigured by an optically induced semiconductor-to-metal transition. *Opt. Express* **2013**, *21*, 10753.
(11) Clark, J. K.; Ho, Y.-L.; Matsui, H.; Delaunay, J.-J. Optically Pumped Hybrid Plasmonic-Photonic Waveguide Modulator Using the VO_2 Metal-Insulator Phase Transition. *IEEE Photonics Journal* **2018**, *10*, 1−9.
(12) Wong, H. M. K.; Yan, Z.; Hallman, K. A.; Marvel, R. E.; Prasankumar, R. P.; Haglund, R. F.; Helmy, A. S. Broadband, Integrated, Micron-Scale, All-Optical Si_3N_4/VO_2 Modulators with pJ Switching Energy. *ACS Photonics* **2019**, *6*, 2734−2740.
(13) Hallman, K. A.; Miller, K. J.; Baydin, A.; Weiss, S. M.; Haglund, R. F. Sub-Picosecond Response Time of a Hybrid VO_2:Silicon Waveguide at 1550 nm. *Adv. Opt. Mater.* **2021**, *9*, No. 2001721.
(14) Parra, J.; Navarro-Arenas, J.; Menghini, M.; Recaman, M.; Pierre-Locquet, J.; Sanchis, P. Low-threshold power and tunable integrated optical limiter based on an ultracompact VO_2/Si waveguide. *APL Photonics* **2021**, *6*, 121301.
(15) Kim, Y.; Wu, P. C.; Sokhoyan, R.; Mauser, K.; Glaudell, R.; Kafaie Shirmanesh, G.; Atwater, H. A. Phase Modulation with Electrically Tunable Vanadium Dioxide Phase-Change Metasurfaces. *Nano Lett.* **2019**, *19*, 3961−3968.
(16) John, J.; Gutierrez, Y.; Zhang, Z.; Karl, H.; Ramanathan, S.; Orobtchouk, R.; Moreno, F.; Cueff, S. Multipolar Resonances with Designer Tunability Using VO_2 Phase-Change Materials. *Physical Review Applied* **2020**, *13*, No. 044053.
(17) Cotrufo, M.; Sulejman, S. B.; Wesemann, L.; Rahman, M. A.; Bhaskaran, M.; Roberts, A.; Alù, A. Reconfigurable image processing metasurfaces with phase-change materials. *Nat. Commun.* **2024**, *15*, 4483.
(18) Hada, M.; Okimura, K.; Matsuo, J. Characterization of structural dynamics of VO_2. *Phys. Rev. B* **2010**, *82*, No. 153401.
(19) Grinolds, M. S.; Lobastov, V. A.; Weissenrieder, J.; Zewail, A. H. Four-dimensional ultrafast electron microscopy of phase transitions. *Proc. Natl. Acad. Sci. U. S. A.* **2006**, *103*, 18427−18431.
(20) Wall, S.; Foglia, L.; Wegkamp, D.; Appavoo, K.; Nag, J.; Haglund, R. F.; Stähler, J.; Wolf, M. Tracking the evolution of electronic and structural properties of VO_2 during the ultrafast photoinduced insulator-metal transition. *Phys. Rev. B* **2013**, *87*, No. 115126.
(21) Lysenko, S.; Rua, A.; Vikhnin, V.; Jimenez, J.; Fernandez, F.; Liu, H. Light-induced ultrafast phase transitions in VO_2 thin film. *Appl. Surf. Sci.* **2006**, *252*, 5512−5515.
(22) Yoshida, R.; Yamamoto, T.; Ishida, Y.; Nagao, H.; Otsuka, T.; Saeki, K.; Muraoka, Y.; Eguchi, R.; Ishizaka, K.; Kiss, T.; Watanabe, S.; Kanai, T.; Itatani, J.; Shin, S. Ultrafast photoinduced transition of an insulating VO_2 thin film into a nonrutile metallic state. *Phys. Rev. B* **2014**, *89*, No. 205114.
(23) Wegkamp, D.; Stähler, J. Ultrafast dynamics during the photoinduced phase transition in VO_2. *Prog. Surf. Sci.* **2015**, *90*, 464−502.
(24) Xu, J.; Chen, D.; Meng, S. Decoupled ultrafast electronic and structural phase transitions in photoexcited monoclinic VO_2. *Sci. Adv.* **2022**, *8*, No. eadd2392.
(25) Wall, S.; Wegkamp, D.; Foglia, L.; Appavoo, K.; Nag, J.; Haglund, R.; Stähler, J.; Wolf, M. Ultrafast changes in lattice symmetry probed by coherent phonons. *Nat. Commun.* **2012**, *3*, 721.
(26) Brady, N. F.; Appavoo, K.; Seo, M.; Nag, J.; Prasankumar, R. P.; Haglund, R. F.; Hilton, D. J. Heterogeneous nucleation and growth dynamics in the light-induced phase transition in vanadium dioxide. *J. Phys.: Condens. Matter* **2016**, *28*, No. 125603.
(27) Kübler, C.; Ehrke, H.; Huber, R.; Lopez, R.; Halabica, A.; Haglund, R. F.; Leitenstorfer, A. Coherent Structural Dynamics and Electronic Correlations during an Ultrafast Insulator-to-Metal Phase Transition in VO_2. *Phys. Rev. Lett.* **2007**, *99*, No. 116401.
(28) Pashkin, A.; Kübler, C.; Ehrke, H.; Lopez, R.; Halabica, A.; Haglund, R. F.; Huber, R.; Leitenstorfer, A. Ultrafast insulator-metal phase transition in VO_2 studied by multiterahertz spectroscopy. *Phys. Rev. B* **2011**, *83*, No. 195120.

(29) Cocker, T. L.; Titova, L. V.; Fourmaux, S.; Holloway, G.; Bandulet, H.-C.; Brassard, D.; Kieffer, J.-C.; El Khakani, M. A.; Hegmann, F. A. Phase diagram of the ultrafast photoinduced insulator-metal transition in vanadium dioxide. *Phys. Rev. B* **2012**, *85*, No. 155120.
(30) Richter, S.; Rebarz, M.; Herrfurth, O.; Espinoza, S.; Schmidt-Grund, R.; Andreasson, J. Broadband femtosecond spectroscopic ellipsometry. *Rev. Sci. Instrum.* **2021**, *92*, No. 033104.
(31) Gutiérrez, Y.; Espinoza, S.; Zahradník, M.; Khakurel, K.; Resl, J.; Cobet, C.; Hingerl, K.; Duwe, M.; Thiesen, P.; Losurdo, M. Characterizing optical phase-change materials with spectroscopic ellipsometry and polarimetry. *Thin Solid Films* **2022**, *763*, No. 139580.
(32) Richter, S.; Herrfurth, O.; Espinoza, S.; Rebarz, M.; Kloz, M.; Leveillee, J. A.; Schleife, A.; Zollner, S.; Grundmann, M.; Andreasson, J.; Schmidt-Grund, R. Ultrafast dynamics of hot charge carriers in an oxide semiconductor probed by femtosecond spectroscopic ellipsometry. *New J. Phys.* **2020**, *22*, No. 083066.
(33) Herrfurth, O.; Richter, S.; Rebarz, M.; Espinoza, S.; Zúñiga-Pérez, J.; Deparis, C.; Leveillee, J.; Schleife, A.; Grundmann, M.; Andreasson, J.; Schmidt-Grund, R. Transient birefringence and dichroism in ZnO studied with fs-time-resolved spectroscopic ellipsometry. *Physical Review Research* **2021**, *3*, No. 013246.
(34) Emminger, C.; Espinoza, S.; Richter, S.; Rebarz, M.; Herrfurth, O.; Zahradník, M.; Schmidt-Grund, R.; Andreasson, J.; Zollner, S. Coherent Acoustic Phonon Oscillations and Transient Critical Point Parameters of Ge from Femtosecond Pump−Probe Ellipsometry. *Phys. Status Solidi RRL* **2022**, *16*, No. 2200058.
(35) Espinoza, S.; Richter, S.; Rebarz, M.; Herrfurth, O.; Schmidt-Grund, R.; Andreasson, J.; Zollner, S. Transient dielectric functions of Ge, Si, and InP from femtosecond pump-probe ellipsometry. *Appl. Phys. Lett.* **2019**, *115*, No. 052105.
(36) Baron, E.; Goldhahn, R.; Espinoza, S.; Zahradník, M.; Rebarz, M.; Andreasson, J.; Deppe, M.; As, D. J.; Feneberg, M. Time-resolved pump−probe spectroscopic ellipsometry of cubic GaN II: Absorption edge shift with gain and temperature effects. *J. Appl. Phys.* **2023**, *134*, No. 075702.
(37) Zahradník, M.; Kiaba, M.; Espinoza, S.; Rebarz, M.; Andreasson, J.; Caha, O.; Abadizaman, F.; Munzar, D.; Dubroka, A. Photoinduced insulator-to-metal transition and coherent acoustic phonon propagation in $LaCo_3$ thin films explored by femtosecond pump-probe ellipsometry. *Phys. Rev. B* **2022**, *105*, No. 235113.
(38) Rensberg, J.; Zhou, Y.; Richter, S.; Wan, C.; Zhang, S.; Schöppe, P.; Schmidt-Grund, R.; Ramanathan, S.; Capasso, F.; Kats, M. A.; Ronning, C. Epsilon-Near-Zero Substrate Engineering for Ultrathin-Film Perfect Absorbers. *Physical Review Applied* **2017**, *8*, No. 014009.
(39) Butakov, N. A.; Knight, M. W.; Lewi, T.; Iyer, P. P.; Higgs, D.; Chorsi, H. T.; Trastoy, J.; Del Valle Granda, J.; Valmianski, I.; Urban, C.; Kalcheim, Y.; Wang, P. Y.; Hon, P. W. C.; Schuller, I. K.; Schuller, J. A. Broadband Electrically Tunable Dielectric Resonators Using Metal−Insulator Transitions. *ACS Photonics* **2018**, *5*, 4056−4060.
(40) Folland, T. G.; Fali, A.; White, S. T.; Matson, J. R.; Liu, S.; Aghamiri, N. A.; Edgar, J. H.; Haglund, R. F.; Abate, Y.; Caldwell, J. D. Reconfigurable infrared hyperbolic metasurfaces using phase change materials. *Nat. Commun.* **2018**, *9*, 4371.
(41) Kats, M. A.; Sharma, D.; Lin, J.; Genevet, P.; Blanchard, R.; Yang, Z.; Qazilbash, M. M.; Basov, D. N.; Ramanathan, S.; Capasso, F. Ultra-thin perfect absorber employing a tunable phase change material. *Appl. Phys. Lett.* **2012**, *101*, 221101.
(42) Vidas, L.; Schick, D.; Martínez, E.; Perez-Salinas, D.; Ramos-Álvarez, A.; Cichy, S.; Batlle-Porro, S.; Johnson, A. S.; Hallman, K. A.; Haglund, R. F.; Wall, S. Does VO_2 Host a Transient Monoclinic Metallic Phase? *Physical Review X* **2020**, *10*, No. 031047.
(43) Gutiérrez, Y.; Vázquez-Miranda, S.; Espinoza, S.; Zhang, Z.; Saiz, J. M.; Ramanathan, S.; Cueff, S. *Time-resolved pump-probe ellipsometry of the photoinduced insulator-metal transition in 25 nm VO2 thin films*; Zenodo, 2024.
(44) Kang, T.; Ma, Z.; Qin, J.; Peng, Z.; Yang, W.; Huang, T.; Xian, S.; Xia, S.; Yan, W.; Yang, Y.; Sheng, Z.; Shen, J.; Li, C.; Deng, L.; Bi, L. Large-scale, power-efficient Au/VO_2 active metasurfaces for ultrafast optical modulation. *Nanophotonics* **2020**, *10*, 909−918.
(45) Cavalleri, A.; Chong, H. H. W.; Fourmaux, S.; Glover, T. E.; Heimann, P. A.; Kieffer, J. C.; Mun, B. S.; Padmore, H. A.; Schoenlein, R. W. Picosecond soft x-ray absorption measurement of the photoinduced insulator-to-metal transition in VO_2. *Phys. Rev. B* **2004**, *69*, No. 153106.
(46) Seoane, J. J.; Parra, J.; Navarro-Arenas, J.; Recaman, M.; Schouteden, K.; Locquet, J. P.; Sanchis, P. Ultra-high endurance silicon photonic memory using vanadium dioxide. *npj Nanophotonics* **2024**, *1*, 37.

https://doi.org/10.1021/acsphotonics.4c01414
ACS Photonics XXXX, XXX, XXX−XXX